Experimental determination and prediction of turbocharger transfer matrix

E. Portier[1], JP. Léandre[2]

1: Centre de Transfert de Technologie du Mans, 20 rue Thalès de Milet 72000 Le Mans
2: Renault CTR, 13 rue Paul Langevin 92359 Le Plessis-Robinson

Abstract: This paper deals with the prediction and the measurement of the 2-port acoustic transfer matrix of the compressor part of a turbocharger. The measurements are performed at several operation points on the compressor map on a dedicated test bench with a two-source method. Predictions and experimental results are compared.

Keywords: turbocharger, acoustical 2-port, transmission loss, prediction, quasi-steady analytical model

1. Introduction

Despite the fact that the turbocharger is now a common part of the intake line, little data in the literature can be used to illustrate the acoustic effect of this sub-system. The reliable researches are mainly found at the KTH in Sweden.

The intake side is generally less equipped with muffler elements than the exhaust side of an engine, therefore the typical noise problems are generally associated with the compressor side. Furthermore, Rämmal and Åbom [1], a few years ago, realized a state of research about acoustic of turbochargers. In their paper the acoustic properties are divided into two parts: a passive part and an active part. The first one is related to the mechanisms of reflexion, transmission and absorption of sound that occur in the compressor in a low frequency range. Below about 1200 Hz, the compressor can be considered as a passive element, like an acoustic filter that will damp and interact with the pressure fluctuations coming from the engine. In higher frequencies, the turbocharger becomes an acoustical source mainly due to the rotating blades of the compressor unit.

For the passive behaviour, the prediction in 1D wave models of intake noise requires the knowledge of the transfer matrices – acoustic 2 ports - of all intake elements. For passive elements, like air filters, pipes, turbocharger exhaust, these matrices are either predicted or measured on dedicated test benches with static conditions (pressure, temperature, flow).

In that context, the KTH built a dedicated test bench to measure acoustic two-port data of turbo-compressors. A description of the testing facility and the experimental procedure are detailed in reference [2]. To this facility, Tiikoja [3] recently improved the acoustical power supplied by applying a phase compensation to the loudspeakers in order to create constructive interference and regulate, in a feedback loop, the electrical power fed to the speakers to achieve the maximum power in each frequency point.

Concerning the prediction, in the low frequency range the plane wave mode dominates, and the acoustic field can be described using linear acoustic 2-port models or 1D gas dynamics models [4]. The 2-port models are able to give quick prediction for small pressure perturbations in ducts whereas the 1D gas dynamics models are usually used to predict wave propagation with high amplitude of pressure fluctuation. Veloso & al. [4] recently presented a non-linear time-domain gas dynamic model to study the acoustic behaviour of both parts of the turbocharger. The simulations of the transmission loss in both directions under zero-flow conditions and under flow condition show a good agreement with the experimental results.

In the first part of this paper (section 2), a brief description of a turbocharger and the associated maps are introduced. Then, in section 3, an analytical model of the compressor part, developed by Renault, is exposed. This model is based on linear 1D equations in permanent conditions which can be used to predict the transfer matrix of the compressor wheel only. This matrix is then extended to the inlet and the outlet of the compressor unit. In order to validate this model, a turbocharger testing facility at Pprime CEAT Poitiers is described in section 4. The section 5 concerns the description of the methodology of the measurement and the description of the experimental results obtained. The last section is dedicated to the comparison between transfer matrixes predicted and measured and the comparison of the intake noise, obtained by using either the measured compressor transfer matrix or the predicted matrix by the analytical model.

2. Turbochargers and compressor maps

Classically, the turbocharger consists of mainly two parts (Figure 1). First, the compressor unit with the compressor wheel and the volute that collects compressed air and drive it to the engine intake and, second, the turbine unit with the turbine housing that collects exhaust gases to the turbine wheel who convert the exhaust energy into shaft power to drive the compressor wheel.

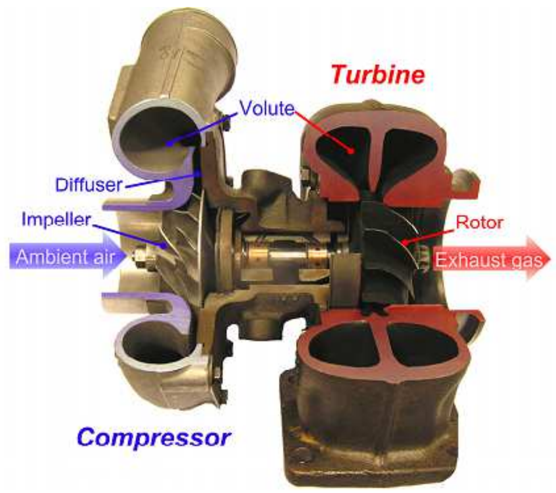

Figure 1 : Turbocharger with a centrifugal compressor and a radial turbine (from Tiikoja [3])

The turbocharger is a singular element which compressor behaviour is described by a pressure/flow rate law and by a efficiency/flow rate law in static conditions and established on specific test bench. These laws are classically presented on a compressor map:

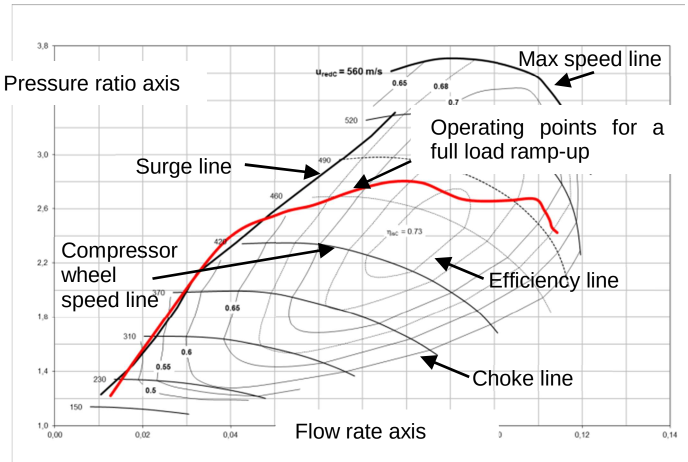

Figure 2 : Typical compressor map

The x-axis is a corrected volume/mass flow rate, the y-axis is either the pressure ratio (absolute outlet pressure divided by the absolute inlet pressure) or the isentropic efficiency. The speed lines are lines of constant speed of the compressor wheel and the maximum speed line limits the compressor map on the top. The left hand boundary is defined as the surge line: at the left of this line, flow instabilities occur and can damage the turbocharger. At the right hand boundary, the choke line represents the limit of efficiency and the region where choke flow conditions can occur. On this compressor map, an example of operating points for a full-load ramp-up is also presented (red curve).

3. Analytical model

The analytical model proposed by Renault was developed by Léandre & Taeko-Nakazato[5].

3.1 Nomenclature

The main variables used in this model are the following:

- Subscripts *e*,*s*: respectively inlet and outlet
- Subscript *t*: absolute, total
- ρ: density (kg/m^{3})
- c: sound velocity (m/s)
- Q: volume flow (m^3/s)
- Q_m: mass flow (kg/s)
- U: flow velocity (m/s)
- T: temperature (K)
- P: pressure (Pa)
- π_c, τ: pressure ratio
- N: RPM of the compressor wheel
- η: efficiency
- $\gamma = C_p/C_v$: compressibility coefficient
- $\dot{W}$: Compression power (W)

3.2 Formulation in permanent flow conditions

In permanent flow conditions, the mass flow rates are the same at the inlet and at the outlet of the compressor:

$$\rho_e Q_e = \rho_s Q_s \qquad [1]$$

Then the conservation of momentum yields to the pressure ratio, function of the reduced flow rate x and the reduced speed of rotation y :

$$\frac{P_{ts}}{P_{te}} = \tau\left(\rho_e Q_e \frac{\sqrt{T_e}}{P_e}, \frac{N}{\sqrt{T_e}}\right) = \tau(x, y) \qquad [2]$$

Finally, the development of the conservation of energy yields to the dimensionless ratio of isentropic efficiency function of the same variables:

$$\eta = \eta\left(\rho_e Q_e \frac{\sqrt{T_e}}{P_e}, \frac{N}{\sqrt{T_e}}\right) \qquad [3]$$

The definition of the isentropic efficiency is the ratio of the power of isentropic compression to the real power of compression:

$$\eta = \frac{\dot{W}_{isentropic}}{\dot{W}} \qquad [4]$$

The use of the first law of thermodynamics leads to the real power of compression:

$$\dot{W} = \dot{M} C_p (T_{ts} - T_{te}) \qquad [5]$$

The absolute temperatures are linked to the static temperatures by:

$$T_t = T + \frac{U^2}{2C_p} \qquad [6]$$

The expression of the isentropic compression power is the same as [5], where T_{ts} is replaced by the following where isentropic compression is assumed:

$$T_{ts} = T_{te} \cdot \left(P_{ts}/P_{te}\right)^{\frac{\gamma-1}{\gamma}} \qquad [7]$$

Finally the isentropic efficiency is obtained:

$$\eta = \frac{\left(P_{ts}/P_{te}\right)^{\frac{\gamma-1}{\gamma}} - 1}{T_{ts}/T_{te} - 1} \qquad [8]$$

and the conservation of energy is expressed as:

$$\frac{\left(P_{ts}/P_{te}\right)^{\frac{\gamma-1}{\gamma}} - 1}{T_{ts}/T_{te} - 1} = \eta\left(\rho_e Q_e \frac{\sqrt{T_e}}{P_e}, \frac{N}{\sqrt{T_e}}\right) = \eta(x, y) \qquad [9]$$

3.3 Small perturbations

The acoustic laws are obtained by using the technique of small perturbations, i.e. by differentiating the previous laws around the medium state:

- For the mass conservation:

$$\frac{\rho_s}{\rho_{s0}} + \frac{Q_s}{Q_{s0}} - \frac{\rho_e}{\rho_{e0}} - \frac{Q_e}{Q_{e0}} = 0 \qquad [10]$$

- For the conservation of momentum:

$$\begin{aligned} &\frac{1}{P_{ts0}} \cdot P_s + \frac{Q_{s0}^2/2S_s^2}{P_{ts0}} \cdot \rho_s + \frac{\rho_{s0} Q_{s0}/S_s^2}{P_{ts0}} \cdot Q_s + \left(-\frac{1}{P_{te0}} + \frac{x_0}{\tau_0}\frac{\partial \tau_0}{\partial x}\frac{1}{2P_{e0}} + \frac{y_0}{\tau_0}\frac{\partial \tau_0}{\partial y}\frac{1}{2P_{e0}}\right) \cdot P_e \\ &- \left(\frac{Q_{e0}^2/2S_e^2}{P_{te0}} + \frac{x_0}{\tau_0}\frac{\partial \tau_0}{\partial x}\frac{1}{2\rho_{e0}} + \frac{y_0}{\tau_0}\frac{\partial \tau_0}{\partial y}\frac{1}{2\rho_{e0}}\right) \cdot \rho_e - \left(\frac{\rho_{e0} Q_{e0}/S_e^2}{P_{te0}} + \frac{x_0}{\tau_0}\frac{\partial \tau_0}{\partial x}\frac{1}{Q_{e0}}\right) \cdot Q_e = 0 \end{aligned} \qquad [11]$$

- For the conservation of energy:

$$\begin{aligned} &\left(\frac{(\gamma-1)/\gamma\left(P_{ts0}/P_{te0}\right)^{\frac{-1}{\gamma}}}{\left(P_{ts0}/P_{te0}\right)^{\frac{\gamma-1}{\gamma}} - 1} \cdot \frac{1}{P_{te0}} - \frac{1}{T_{ts0}/T_{te0} - 1} \cdot \frac{T_{s0}}{T_{te0} P_{s0}}\right) \cdot P_s \\ &+ \left(\frac{(\gamma-1)/\gamma\left(P_{ts0}/P_{te0}\right)^{\frac{-1}{\gamma}}}{\left(P_{ts0}/P_{te0}\right)^{\frac{\gamma-1}{\gamma}} - 1} \cdot \frac{Q_{s0}^2/2S_s^2}{P_{te0}} + \frac{1}{T_{ts0}/T_{te0} - 1} \cdot \frac{T_{s0}}{T_{te0}\rho_{s0}}\right) \cdot \rho_s \\ &+ \left(\frac{(\gamma-1)/\gamma\left(P_{ts0}/P_{te0}\right)^{\frac{-1}{\gamma}}}{\left(P_{ts0}/P_{te0}\right)^{\frac{\gamma-1}{\gamma}} - 1} \cdot \frac{\rho_{s0} Q_{s0}/S_s^2}{P_{te0}} - \frac{1}{T_{ts0}/T_{te0} - 1} \cdot \frac{Q_{s0}}{S_s^2 C_p T_{te0}}\right) \cdot Q_s \\ &+ \left(\frac{(\gamma-1)/\gamma\left(P_{ts0}/P_{te0}\right)^{\frac{-1}{\gamma}}}{\left(P_{ts0}/P_{te0}\right)^{\frac{\gamma-1}{\gamma}} - 1} \cdot \frac{-P_{ts0}}{P_{te0}^2} + \frac{T_{ts0}/T_{te0}}{T_{ts0}/T_{te0} - 1} \cdot \frac{T_{e0}}{T_{te0} P_{e0}} + \frac{x_0}{\eta_0}\frac{\partial \eta_0}{\partial x}\frac{1}{2P_{e0}} + \frac{y_0}{\eta_0}\frac{\partial \eta_0}{\partial y}\frac{1}{2P_{e0}}\right) \cdot P_e \\ &+ \left(\frac{(\gamma-1)/\gamma\left(P_{ts0}/P_{te0}\right)^{\frac{-1}{\gamma}}}{\left(P_{ts0}/P_{te0}\right)^{\frac{\gamma-1}{\gamma}} - 1} \cdot \frac{-P_{ts0}}{P_{te0}} \cdot \frac{Q_{e0}^2/2S_e^2}{P_{te0}} - \frac{T_{ts0}/T_{te0}}{T_{ts0}/T_{te0} - 1} \cdot \frac{T_{e0}}{T_{te0}\rho_{e0}} - \frac{x_0}{\eta_0}\frac{\partial \eta_0}{\partial x}\frac{1}{2\rho_{e0}} - \frac{y_0}{\eta_0}\frac{\partial \eta_0}{\partial y}\frac{1}{2\rho_{e0}}\right) \cdot \rho_e \\ &+ \left(\frac{(\gamma-1)/\gamma\left(P_{ts0}/P_{te0}\right)^{\frac{-1}{\gamma}}}{\left(P_{ts0}/P_{te0}\right)^{\frac{\gamma-1}{\gamma}} - 1} \cdot \frac{-P_{ts0}}{P_{te0}} \cdot \frac{\rho_{e0} Q_{e0}/S_e^2}{P_{te0}} + \frac{T_{ts0}/T_{te0}}{T_{ts0}/T_{te0} - 1} \cdot \frac{Q_{e0}}{S_e^2 C_p T_{te0}} - \frac{x_0}{\eta_0}\frac{\partial \eta_0}{\partial x}\frac{1}{Q_{e0}}\right) \cdot Q_e = 0 \end{aligned} \qquad [12]$$

3.4 Transfer matrix of the compressor wheel

These last equations yield the following matrix relation:

$$\begin{pmatrix} P_s \\ \rho_s \\ Q_s \end{pmatrix} = [M] \cdot \begin{pmatrix} P_e \\ \rho_e \\ Q_e \end{pmatrix} \qquad [13]$$

Where [M] is a 3x3 square matrix.

The last step consists in writing the usual transfer matrix of order 2.

By assuming a reversible adiabatic transformation at the inlet of the compressor ($P_e = \rho_e c_e^2$), the matrix [M] is reduced to a 3x2 matrix:

$$\begin{pmatrix} P_s \\ \rho_s \\ Q_s \end{pmatrix} = \begin{bmatrix} M_{11} + M_{12}/c_e^2 & M_{13} \\ M_{21} + M_{22}/c_e^2 & M_{23} \\ M_{31} + M_{32}/c_e^2 & M_{33} \end{bmatrix} \cdot \begin{pmatrix} P_e \\ Q_e \end{pmatrix} \qquad [14]$$

Finally, by removing the line corresponding to ρ_s, the usual transfer matrix is obtained:

$$\begin{pmatrix} P_s \\ Q_s \end{pmatrix} = \begin{bmatrix} M_{11} + M_{12}/c_e^2 & M_{13} \\ M_{31} + M_{32}/c_e^2 & M_{33} \end{bmatrix} \cdot \begin{pmatrix} P_e \\ Q_e \end{pmatrix} \qquad [15]$$

As the main assumption is relative to quasi-steady conditions, the model obtained at this stage is not frequency dependent.

Furthermore, the pressure ratio τ, the efficiency η and their first partial derivatives (with respect to x and y) have to be interpolated in the corresponding maps at the operating points considered. For this, up to 9 interpolation algorithms have been tested by Renault before finding the best.

Lastly, the inlet and outlet quantities are expressed in relation with the flow direction. Because the pursued acoustic propagation is opposite for the compressor part (from the engine to the intake), the final transfer matrix is obtained by inverting the matrix [15].

3.5 Transfer matrix of the compressor unit

The previous model is built with laws governing the behaviour of the compressor at the inlet and at the outlet of the compressor wheel. In order to compare with experimental data, the transfer matrix of the wheel must be spread at the inlet and at the outlet of the compressor unit.

Schematically, the compressor unit can be divided in several parts:

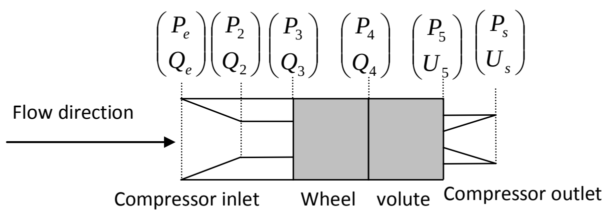

Figure 3 Decomposition of the compressor unit

In a matrix format, the global transfer matrix is:

$$\begin{pmatrix} P_s \\ Q_s \end{pmatrix} = [T_{divergent}]*[T_{volute}]*[T_{wheel}]*[T_{straight\_duct}]*[T_{convergent}]*\begin{pmatrix} P_e \\ Q_e \end{pmatrix} \qquad [16]$$

With:

- $[T_{divergent}]$: the transfer matrix of the divergent cone at the outlet of the compressor with flow;
- $[T_{volute}] = \begin{pmatrix} 1 & 0 \\ -\frac{j\omega V}{\rho c^2} & 1 \end{pmatrix}$: the transfer matrix of the volute of volume V;
- $[T_{wheel}]$: the transfer matrix of the wheel (eq.[15] inverted);
- $[T_{straight\_duct}]$: the transfer matrix of a straight duct with flow;
- $[T_{convergent}]$: the transfer matrix of a convergent cone at the inlet of the compressor with flow.

Because the previous matrixes are frequency-dependent, the transfer matrix extended to the inlet and to the outlet of the compressor part becomes also frequency-dependent.

4. Experimental Set-Up

4.1 Test Bench

For the present study, the test bench for turbocharger at Pprime CEAT at Poitiers (France) is used and modified for acoustic transfer measurement purposes.

Figure 4 Turbocharger test facility at Pprime CEAT

Compressed air from a network of 200 bars is first expanded to a pressure of several bars and converted to flow rate by using a sonic nozzle. This flow rate (up to 100g/s) is then heated by an electric heater of 54kW (maximum of 650℃) in order to drive the turbocharger turbine. A lubrication rig with pressure adjustment and electric heater is also provided to ensure lubrication and cooling of the connecting rod and of the bearings of the turbocharger.

The air compressed by the turbocharger is controlled in the downstream section by a load throttle (butterfly valve). The flow mass in the compressor part is measured by a Venturi tube and the test facility is equipped with pressure and temperature probes in all parts to survey the process.

4.2 Turbocharger

The turbocharger tested in this study was the one of the H4JT engine (Figure 5). The inlet and outlet diameters are respectively 45mm and 32mm.

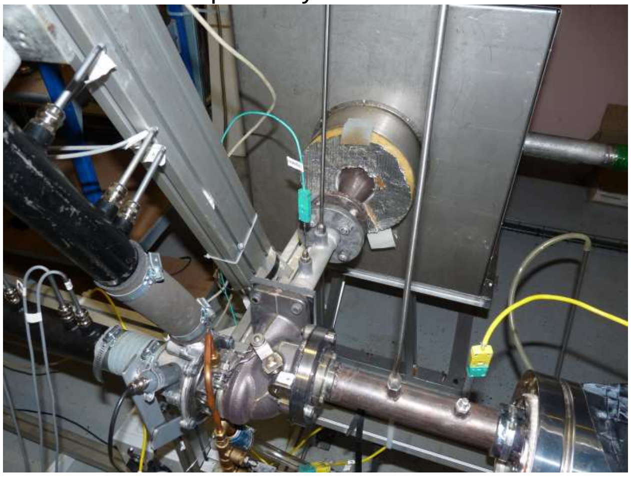

Figure 5 : Turbocharger set-up

4.3 Acoustic adjustments

The compressor unit is equipped for acoustic measurements: four ¼" microphones Bruël & Kjaer (type 4938) in the upstream part (Figure 6) and three water cooled PCB dynamic pressure transducers (type 106B52) in the downstream part (Figure 7).

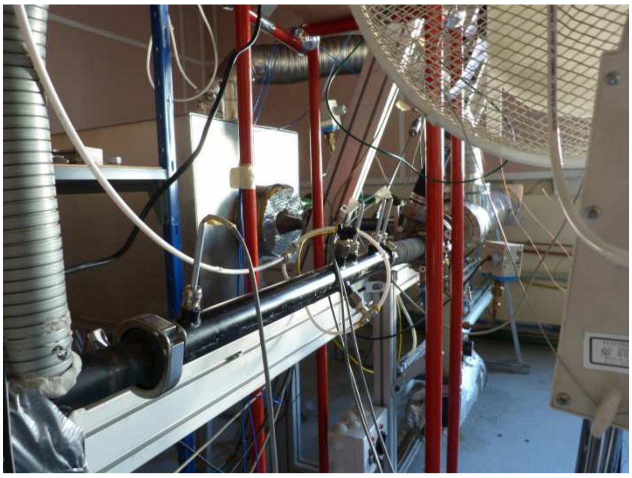

Figure 6 : Upstream microphones

Due to high pressure and temperature in the downstream side, the transducers are specially designed and chosen to have the larger sensitivity.
The distances between the pressure probes are chosen to limit the indefinite frequencies and to obtain sufficient phase shift for low frequency measurement. Four locations are determined as follows and used for the two pressure measurement ducts:

Δ (µ1 – µ2)	Δ (µ1 – µ3)	Δ (µ1 – µ4)
30	100	505

Table 1 Separation locations

Because only three transducers are used in the downstream part, the most spread out locations are used in order to perform measurements from 100 Hz.
To match the diameters of inlet and outlet of the compressor, a duct of 45mm diameter is used in the upstream part and a duct of 35mm diameter is used on the other side.

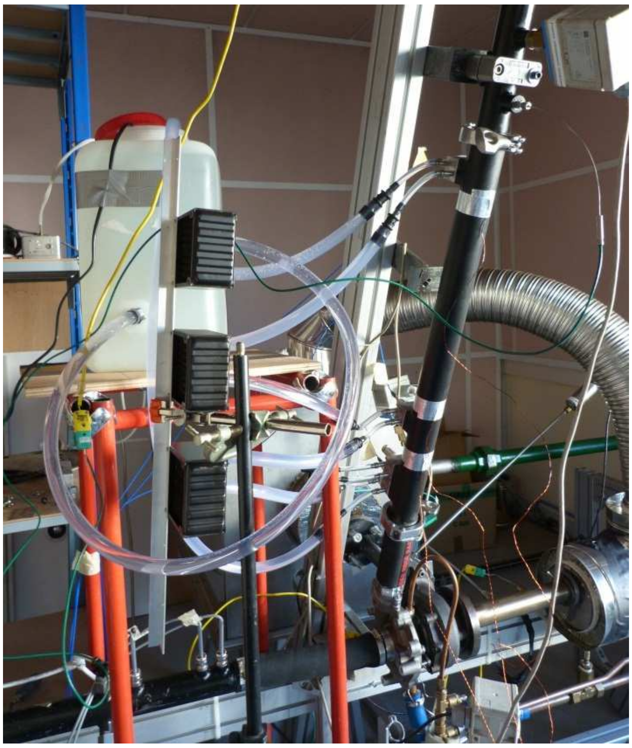

Figure 7 : Set-up in the downstream part

Concerning the acoustical sources, in order to support the small negative pressure in the upstream side and high positive pressure (up to 3 bars) in the downstream side, a balance of the pressure at both side of the diaphragm of the speaker is performed inside the enclosure. Furthermore, one of the two sources is specially designed to support high temperature in the downstream part: the three modes of thermal propagation are treated. The conduction, by metallic duct, is blocked by an insulating rig of Peek material, the convection is non-existent because all the pressure leakage are treated and, finally, the thermal radiation is eliminated by moving away the loudspeaker from the hot flow (Figure 8).

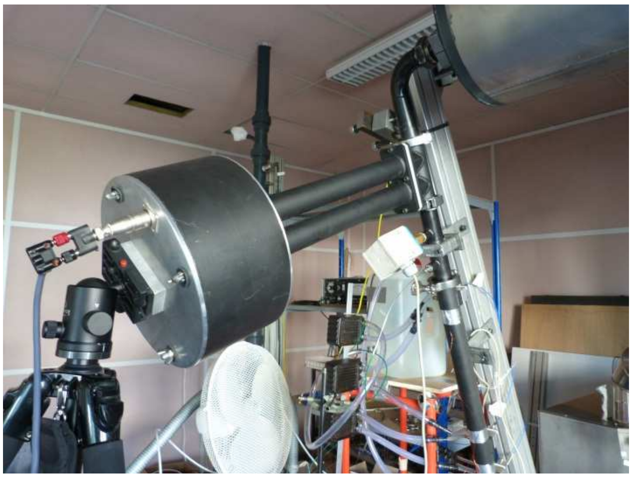

Figure 8 : Downstream source

To insure the best signal-to-noise ratio during the measurements, the geometry in front of the diaphragm is specially designed so as to obtain the maximum acoustic power. The frequency response in anechoic conditions at both sides with a step sine excitation under 26 Volts RMS is the following:

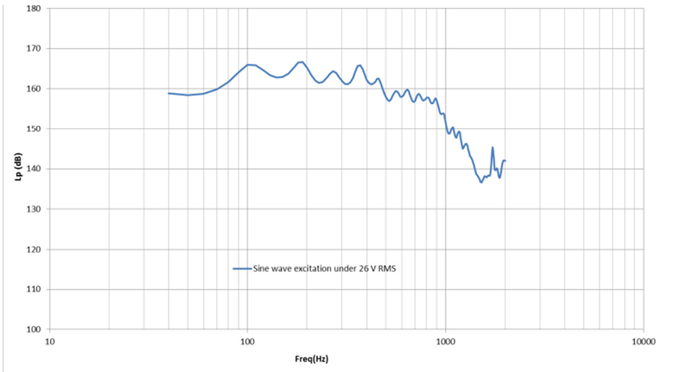

Figure 9 : Acoustic response of the source with anechoic terminations under 26 Volts step sine excitation.

Finally, in order to limit acoustic reflection in the downstream side, a specific anechoic termination was designed:

Figure 10 : Anechoic silencer

The reflection coefficient as a function of the frequency obtained is as followed:

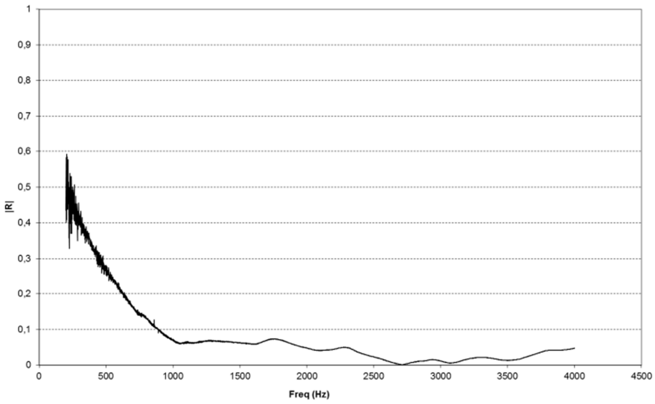

Figure 11 : Anechoic termination response

It is important to note that smaller reflection coefficients can be obtained at low frequencies with this kind of termination (|R|<0.2 for f<200 Hz). See for this reference [6].

5. Experimental results

5.1 Transfer matrix measurements

The compressor is characterized by its scattering matrix obtained with an incoming and outcoming wave decomposition:

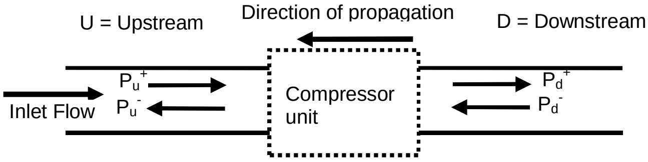

Figure 12 : A two-port acoustic system

The scattering matrix is composed of four elements, two complex transmission coefficients and two complex reflection coefficients:

$$\begin{pmatrix} P_d^+ \\ P_u^- \end{pmatrix} = \begin{pmatrix} T^+ & R^- \\ R^+ & T^- \end{pmatrix} \begin{pmatrix} P_u^+ \\ P_d^- \end{pmatrix} \qquad [17]$$

The two transmission coefficient T^+ and T^- are relevant to the transmission loss coefficients of the two directions of acoustic propagation.

Two independent states are necessary to fully determine this system. A two sources method is employed to ensure the independency of the two states.

This matrix is then transformed into a transfer matrix formulation for comparison with the analytical model exposed above.

5.2 Operational points

For the compressor studied (H4JT), 16 operational points are chosen on the full-load ramp-up curve, 7 on the deceleration curve and 3 in the middle of the map (Figure 13). The first point is relative to the stationary turbocharger.

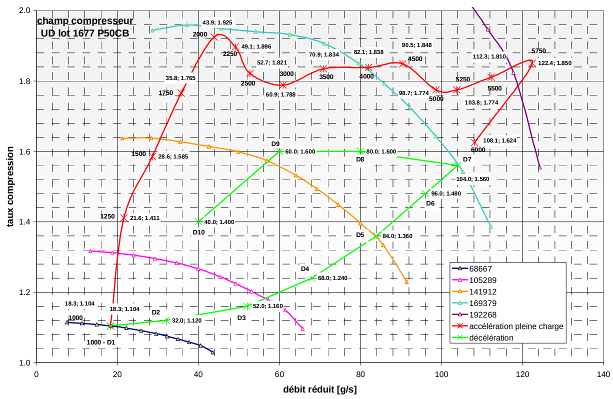

Figure 13 : Operating points

5.3 Experimental design

For each operating point, a step sine measurement is performed from 100 to 1200 Hz by steps of 10Hz for the two configurations (for each acoustic source activated). The coherence function allows the estimation of the quality of the transfer function acquired. In addition, the temperature gradient, on the downstream part, is measured at the three locations of the pressure transducers. Thus, the decrease of the temperature along the measurement duct is specifically treated and added in the data processing.

5.4 Results

First, the transmission loss (TL) coefficients in the upstream direction (toward the air inlet in a car) are presented (Figure 14). When the turbocharger is turning off, a peak of attenuation is observed around 1050Hz. In the literature, this peak is often related to the Hershel-Quincke effect, i.e. a destructive interference in the propagation path [2]. This peak also occurs in operation and seems to be at the same frequency location whereas Rämmal & al. [2] observed a shift towards low frequencies with a KKK2474 turbocharger. Furthermore, in the frequency range below the attenuation peak, the TL increases with flow or with the pressure ratio. The TL coefficients on the downstream direction (toward the engine) show that the acoustic behaviour of the compressor is not symmetric (Figure 15). As for the previous case, a peak also occurs at the same frequency when the turbocharger is in the stationary state, but almost disappears when the turbocharger is functioning. Furthermore, in that direction the TL does not change with flow or pressure ratio and the levels (less than 5 dB) indicate that the compressor is quite acoustically transparent.

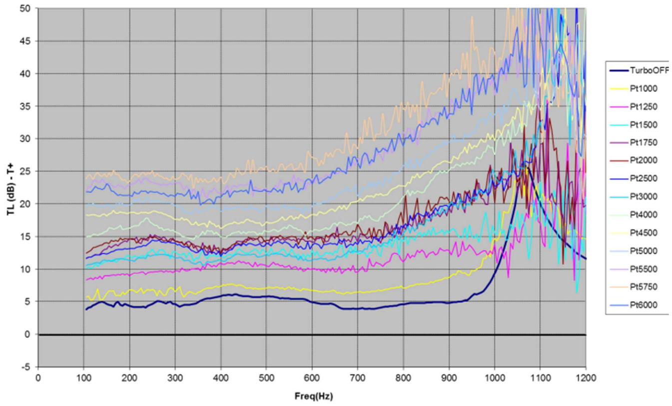

Figure 14 Upstream TL (toward air inlet)

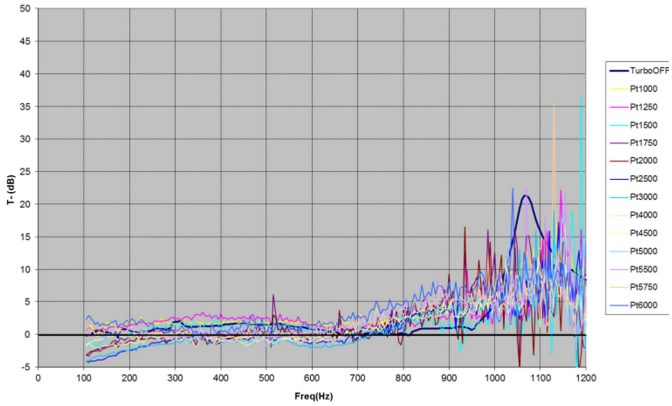

Figure 15 Downstream TL (toward engine)

6. Comparisons with model

In this section, comparisons are achieved between transfer matrixes obtained with the model and with the experimental data.

6.1 Reduction of the transfer matrixes

All the transfer matrixes are in the form:

$$\begin{pmatrix} P_s \\ Q_s \end{pmatrix} = [T] \begin{pmatrix} P_e \\ Q_e \end{pmatrix} = \begin{bmatrix} T_{11} & T_{12} \\ T_{21} & T_{22} \end{bmatrix} \begin{pmatrix} P_e \\ Q_e \end{pmatrix} \qquad [18]$$

The terms T_{11} and T_{22} are dimensionless, while the term T_{21} has the dimension of an admittance and the term T_{12} the dimension of an impedance. In order to compare all the terms in the same graph, these terms are turned dimensionless by using the characteristic impedances of the media at the inlet and at the outlet of the compressor: $Z_{ce} = \rho_e c_e / S_e$ and $Z_{cs} = \rho_s c_s / S_s$. To avoid confusion between conventions, we use an average characteristic impedance:

$$Z_{cm} = \sqrt{Z_{ce}.Z_{cs}} \qquad [19]$$

All the matrixes – i.e. experimental and simulated - are thus reduced into the following form:

$$[T]_{red} = \begin{bmatrix} T_{11} & T_{12} / Z_{cm} \\ T_{21}.Z_{cm} & T_{22} \end{bmatrix} \qquad [20]$$

6.2 Influence of extending the predicted matrixes

First, the predicted data without extending the transfer matrix, i.e. the transfer matrix of the wheel only, is compared with the experimental data at the first operating point (Figure 16).
The graph on the left presents the modulus of the elements of the matrixes and the one of the right, the phases of the elements. The pressure elements T_{11} and T_{22} are respectively in blue and red colours, the reduced term T_{12} is in green colour and the reduced term T_{21} is in black colour. Finally, the predicted quantities are plotted in dashed line and the measured data in solid line.
As the acoustic model is not frequency-dependant, the predicted quantities are all constant in the frequency range. At this step, one can observe that the moduli are similar and obviously the phases are uncorrelated with the experimental data.

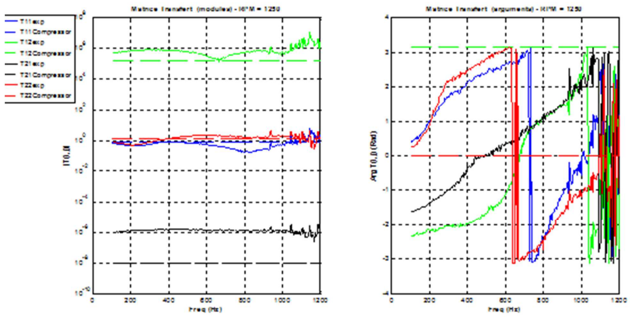

Figure 16 Comparison of the unspread predicted matrix with experimental data (Pt 1250 RPM)

When the transfer matrix of the wheel is extended to the inlet and outlet of the compressor unit, the quantities become frequency-dependant, and one can observe a better correlation between modulus quantities (Figure 17). In addition, the phases are fitted more precisely in low frequencies but the shifts do not occur at the same frequency locations.

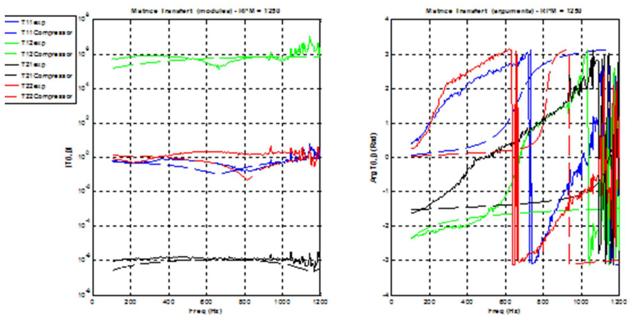

Figure 17 Comparison of the spread predicted matrix with experimental data (Pt 1250 RPM)

6.3 Other operating points

Two other results are displayed here: one for the operating point near the surge curve at the highest pressure ratio (Figure 18) and the other for the operating point corresponding to the highest flow rate (Figure 19).

In the first case, the same remarks can be observed as in the previous comparison. Concerning the point with high flow rate the results on the moduli seem to be less accurate.

Thus, for all operating points the phases are poorly predicted. One of the reasons for this is that the acoustic propagation model on the convergent and divergent cones should be better validated with flow. In addition, some acoustic resonances are not accurately located frequency-wise, which may be explained by the rough approximation of the volume of the volute and the dead volume in the geometry of the compressor unit which is not accounted for.

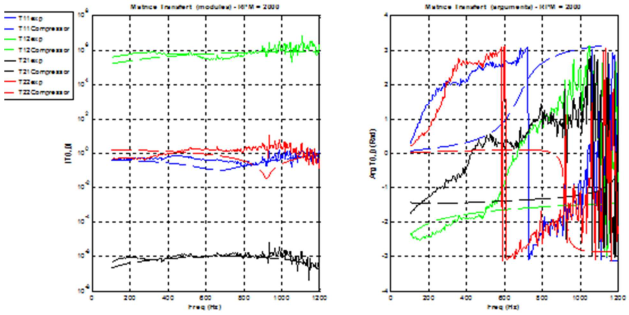

Figure 18 Pt 2000 RPM

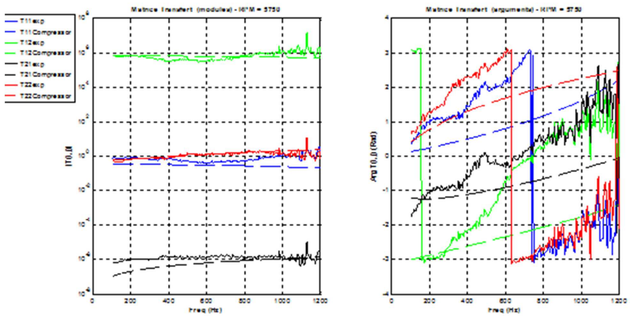

Figure 19 Pt 5750 RPM

6.4 Effect on the intake noise

Lastly, some comparisons are performed on the intake noise between experimental data obtained on vehicle and predicted data obtained with the 1D software SAPPY developed by Renault.

To this end, all the elements of the air intake system from the cylinders to the air inlet are modelled by their own transfer matrix (impedance matrix) available with Sappy. Figure 20 shows an example of the intake model realized with Sappy where the compressor matrix either comes from the previous model or comes from the actual measurements.

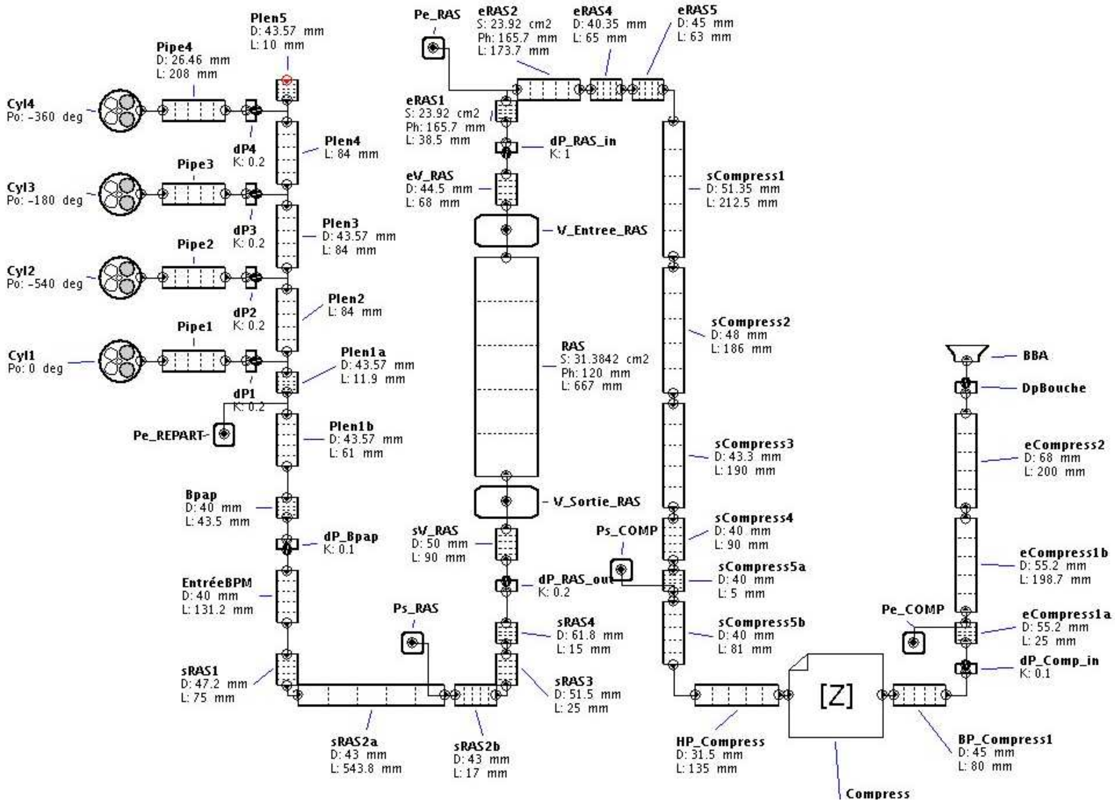

Figure 20 Example of intake modelisation by Sappy

Figure 21 to Figure 24 present the results for H2-H4-H6 and H8 computations. The predicted values are either calculated with the analytical model of the compressor (on the left side) or with the experimental data injected into the 1D calculation (on the right side). The experimental values of the intake noise are plotted in dashed line.
It is noted that the predictions with the 1D software are more accurate with the transfer matrices measured than with the matrices predicted by the analytical model.

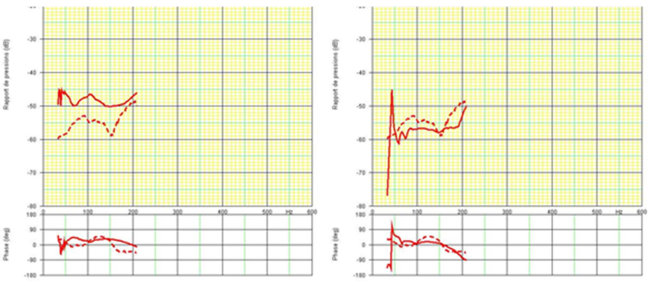

Figure 21 H2 intake noise

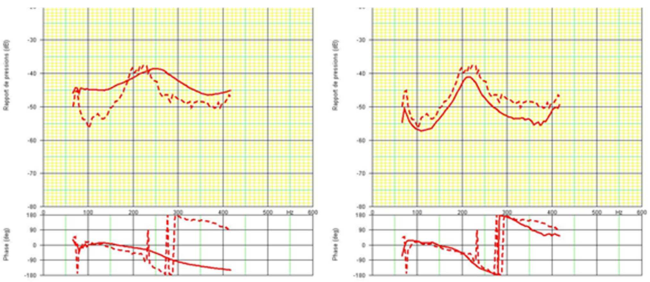

Figure 22 H4 intake noise

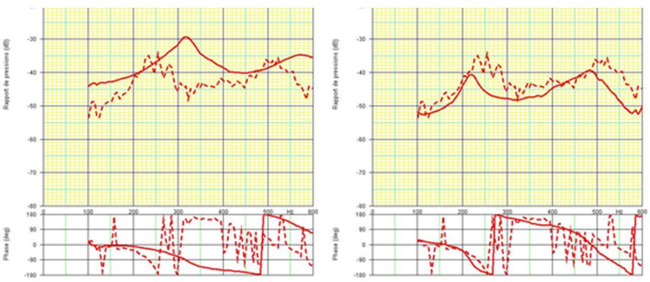

Figure 23 H6 intake noise

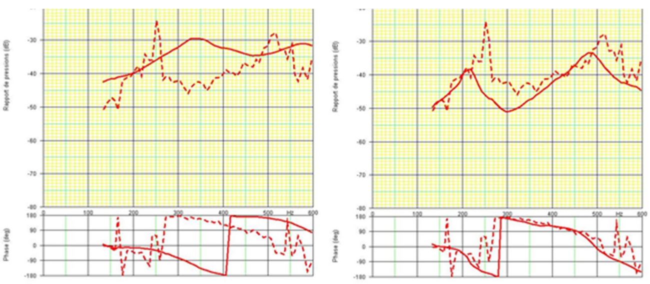

Figure 24 H8 intake noise

7. Conclusion

In this paper, an analytical model established by Renault is presented and used to compute the transfer matrix of the compressor unit of a turbocharger.
In addition, a test bench is presented and modified for acoustic measurements. Dedicated acoustic sources are provided and special procedures are employed to take into account, for example, the temperature gradient in the downstream side of the compressor.
Comparisons are performed between experimental data and the transfer matrices provided by the analytical model and show notable discrepancies. In the present state of modelling, only the measured matrices can be used for intake noise prediction.

The actual quasi steady model for the compressor is inadequate. Intuitively, the compressor wheel should introduce an inertial term in the equation of conservation of momentum that must be corrected. In contrast, the mass conservation would not change as the capacitive effect of the wheel is small compared to the volume of air intake system.
A 1D model of sliced radial propagation in the compressor wheel will be studied and parameters of friction and heat exchange will be introduced into the model.

In the meantime, given the good results of calculated intake noise with a compressor characterized experimentally, Renault has decided to measure five other compressors with CTTM and thus begin to build a database of impedance matrices of compressors.

8. References

[1] H. Rämmal, M Åbom “Acoustics of turbochargers” SAE Technical Paper 2007-01-2205

[2] H. Rämmal, M Åbom “Experimental determination of sound transmission in turbo-compressors” SAE Technical Paper 2009-01-2045

[3] H. Tiikoja, “Acoustic characterization of turbochargers and pipe terminations”, Licenciate Thesis 2012, KTH CCGEx, Stockholm, Sweden

[4] R. Veloso & al., “Simulation of sound transmission through automotive turbochargers”, SAE Technical Paper 2012-01-1560

[5] A. Taeko-Nakazato, "Modélisation du compresseur centrifuge dans le logiciel SAPPY", Stage Bac+5 2009 ISTIL

[6] E. Portier, JP. Dalmont, " Acoustic optimization of anechoic termination with and without superimposed flow”, 7th Symposium SIA / CTTM "Automobile and Railroad Comfort – Acoustics, Vibrations & Thermal issues", Le Mans, October 24 & 25, 2012